AGU INTERNATIONAL JOURNAL OF SCIENCES
ISSN 0866 - 8086

# DENSITY FUNCTIONAL THEORY STUDY OF NITRIC OXIDE ADSORPTION ON AN ELECTRON-RICH Pd4 CLUSTER SUPPORTED BY $SrTiO_{3-\delta}$

Pham Ngoc Thanh[1]
[1]*An Giang University, VNU-HCM*

***Information:***
*Received: 19/06/2024*
*Accepted: 14/10/2024*
*Published: 12/2024*

***Keywords:***
*Climate change, NOx purification, density functional theory (DFT)*

## ABSTRACT

*Nitrogen oxide (NOx) emissions from human activities have led to significant negative impacts, including air pollution, photochemical smog, and respiratory health problems. Additionally, NOx emissions contribute to the greenhouse effect, exacerbating climate change. To address these effects, NOx purification catalysis has been developed. Among promising candidates for NOx purification catalysts, strontium titanate-supported palladium (Pd) shows great potential. However, the adsorption mechanism of NO on this catalyst remains elusive. This study aims to clarify the NO adsorption mechanism using density functional theory (DFT) calculations by investigating NO adsorption on a Pd4 cluster supported by an oxygen-deficient SrTiO3(001) surface. Our findings reveal that NO is strongly adsorbed on the $Pd_4$ cluster, with the strong interaction originating from a back-donation process from Pd d-states to the NO 2π* orbitals.*

## 1. INTRODUCTION

$NO_x$ emission has various negative impacts on our environments, e.g., air pollution, photochemical smog, acid rain, and respiratory health problems. (Granger & Parvulescu, 2011) Moreover, it was found that $NO_x$ emissions contribute to the greenhouse effect, worsening climate change (Lammel & Graßl, 1995). $NO_x$ gases are classified as indirect greenhouse gases because they react with other trace gases, leading to absorption in the spectral range relevant to the greenhouse effect (infrared wavelengths). The primary source of NOx emissions is fossil fuel combustion. Therefore, developing catalytic methods for NOx purification, such as three-way catalysts or selective catalytic reduction, to mitigate NOx emissions from fossil fuel combustion, is of significant interest.

In practice, NOx purification catalysts are typically composed of platinum-group metal (PGM) nanoparticles supported on high-surface-area oxides, such as CeO2 and Al2O3. However, because PGMs are scarce and expensive, reducing their usage in the NOx purification catalysts is of practical importance. Furthermore, under working conditions of high temperature and pressure, metal nanoparticles can easily become deactivated due to agglomeration (sintering) (Goodman et al., 2019). Sintering leads to a decrease in specific surface area and, consequently, a reduction in catalytic activity. As a result, conventional NOx purification catalysts require an excess amount

of PGMs to mitigate thermal deactivation. To overcome this issue, several strategies have been proposed, and among them, the development of new support oxides to effectively anchor PGM nanoparticles has received significant attention (Demizu et al., 2017; Spezzati et al., 2017; Su et al., 2017; Wang et al., 2021).

Recently, strontium titanate-supported Pd catalyst (Pd/STO) is realized as an efficient $NO_x$ purification catalyst (Beppu et al., 2018; Demizu et al., 2017). It was found that strontium titanate -supported Pd catalyst has not only a high catalytic activity of the NO conversion but also an excellent thermal stability against sintering. Beppu et al fabricated the Ti-rich $SrTi_xFe_{1-x}O_{3-\delta}$-supported Pd catalyst and found that the catalytic activity of NO reduction is much higher than conventional $Pd/Al_2O_3$ catalyst catalyst (Beppu et al., 2018). Moreover, the sintering resistance of $Pd/SrTi_xFe_{1-x}O_{3-\delta}$ is always higher than $Pd/\gamma$-$Al_2O_3$. However, $Pd/SrTi_xFe_{1-x}O_{3-\delta}$ suffers from the deactivation in an oxidative atmosphere. To mitigate the deactivation in oxidative atmosphere, we propose to use $Sr_3Ti_2O_7$ in a Ruddlesden–Popper phase as the oxide support (Pham et al., 2024). It was found that rock-salt SrO layer effectively hinders the Pd ions penetration into bulk region of $Sr_3Ti_2O_7$, thus maintaining Pd nanoparticles are highly anchored even under oxidative atmosphere.

However, the interaction between nitric oxide (NO) and Pd/STO remains unknown. The interaction between NO and Pd/STO is particularly important because it was found that the active site for NO reduction is the three-phase boundary among gas (NO), metal nanoparticle (Pd) and oxide support (Fujiwara et al., 2020; Hirakawa et al., 2021) . As the first step toward a full elucidation of NO reduction on Pd/STO, we herein evaluate the mechanism of NO adsorption on Pd/STO catalyst by studying NO adsorption on $Pd_4$ supported on SrO-terminated O-deficient $SrTiO_3$(001) slab model using density functional theory (DFT) method. The preferable adsorption sites of NO were found. Electronic structure analysis was carried out to provide atomistic insights into the NO adsorption.

## 2. METHODOLOGY

All our spin-polarized DFT calculations were performed by using Quantum ESPRESSO package (Giannozzi et al., 2017). The interactions between core ions and valance electrons were described by the ultrasoft pseudopotential method (Vanderbilt, 1990). The valance electron was expanded by a plane wave basis with the kinetic cut-off energies for wave function and augmented charge density of 50 Ry and 400 Ry, respectively. The exchange correlation energy was elucidated by revised Perdew-Burke-Ernzerhof (RPBE) functional proposed by Hammer and co-workers (Hammer et al., 1999). The dispersion interaction was taken into account by using the dispersion correction by Grimme et al (RPBE+D3) (Grimme et al., 2010). The RPBE+D3 method has been shown to provide accurate descriptions for several adsorption and reaction systems, including NO adsorption and reduction on Cu catalysts (Al Fauzan et al., 2023; Pham et al., 2020). To mitigate the delocalization error of the Ti 3*d* state, we employ Hubbard *U* correction with effective *U* for Ti 3*d* of 5 eV(Pham et al., 2024).

The $Pd_4$/STO catalyst is modeled by a small $Pd_4$/ cluster supported on oxygen-deficent $SrTiO_3$ (001) surface. The oxygen-deficient $SrTiO_3$ (001) surface is represented by using a SrO-terminated three-layer $SrTiO_3$(001) slab with a periodicity of $p(3\times3)$ and single oxygen vacancy ($V_O$) at the topmost layer are employed (Figure 1). The vacuum thickness of 16 Å was introduced along surface normal direction. This system is hereafter referred as STO+$V_O$. The

most stable geometry of $Pd_4$ on STO+$V_O$ ($Pd_4$/STO+$V_O$) is optimized by using machine-learning enhanced global optimization (Pham et al., 2024).

A single NO is adsorbed on one side of the $Pd_4$/STO+$V_O$ slab with several adsorption sites and geometries. Structural optimizations were carried out $V_O$ until the total force acting on atoms are less than 0.05 Ry/Bohr$^{-1}$, while the bottommost SrO layer was kept fixed at its bulk positions. The Brillouin zone integration was sampled by a 3 × 3 × 1 uniform k-point mesh. Long range spurious multipole interactions along surface normal direction were eliminated by an effective screening medium (ESM) method (Otani & Sugino, 2006).

## 3. RESULTS AND DISCUSSION

### *3.1 Structure of $Pd_4$/STO+$V_O$ and charge states of the supported $Pd_4$ cluster*

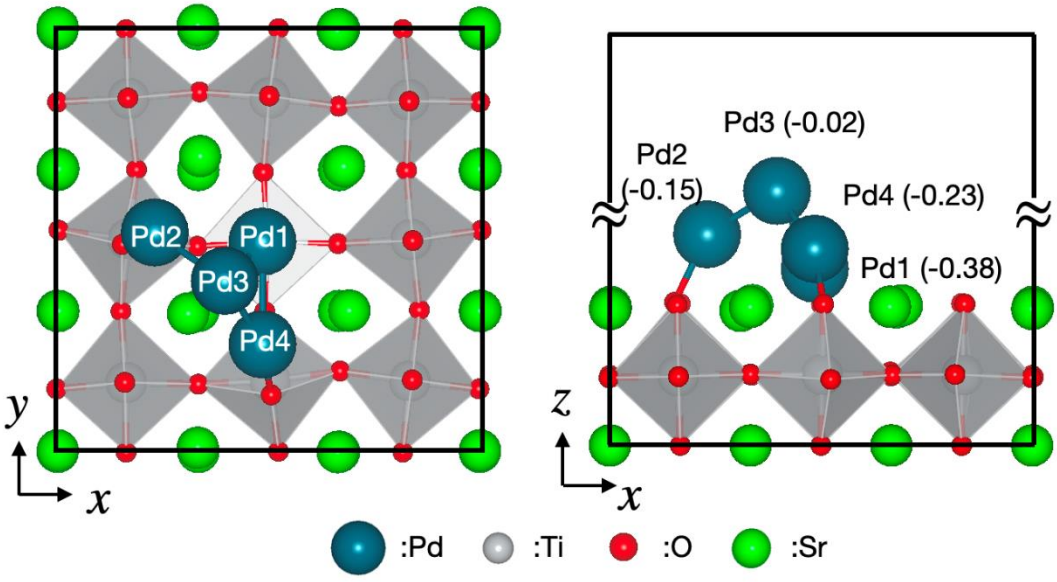


**Figure 1. Top and side views of $Pd_4$/STO+$V_O$ slab model. The values in parenthesis show the effective charge $q$ of Pd atoms, which is estimated as $q = q_L - Z$, where $q_L$ and Z are total electron population using Löwdin population analysis and total number of valence electrons of Pd, respectively**

The atomic model of $Pd_4$/STO+$V_O$ is shown in Figure 1. The $Pd_4$ cluster adopts a distorted tetrahedral geometry due to strong interactions with the STO+$V_O$ substrate. In this model, we define interface Pd atoms as those bonded to oxygen atoms from the substrate—specifically, Pd1, Pd2, and Pd4. Meanwhile, Pd3 is considered a noninterface atom, as it has no direct bond with the substrate. Estimated average Pd-Pd bond length among interface atoms and that between the interface and noninterface Pd atoms are 3.50 and 2.66 Å, respectively. The former is significantly larger, while the latter is slightly smaller than the typical Pd-Pd bond length in fcc Pd (2.75 Å).

Löwdin population analysis (Giannozzi et al., 2017) indicates that the $Pd_4$ cluster is negatively charged upon adsorption on STO+$V_O$, with a total charge of −0.79 $e$, showing that electron donation occurs from the substrate to $Pd_4$, making the cluster electron-rich. From Figure 1, it can be seen that this electron donation is not distributed homogeneously over the Pd cluster. Only the interface Pd atoms (Pd1, Pd2, Pd4) are

negatively charged, while the non-interface Pd atom (Pd3) remains almost neutral. Among the interface Pd atoms, the electron donation is also unevenly distributed. The Pd atom directly connected to the oxygen vacancy (Pd1) has the strongest electron donation, resulting in its most negatively charged state of −0.38 e, while the other Pd atoms have effective charge states of −0.15 and −0.23 e.

### *3.2 NO adsorption on $Pd_4/STO+V_O$*

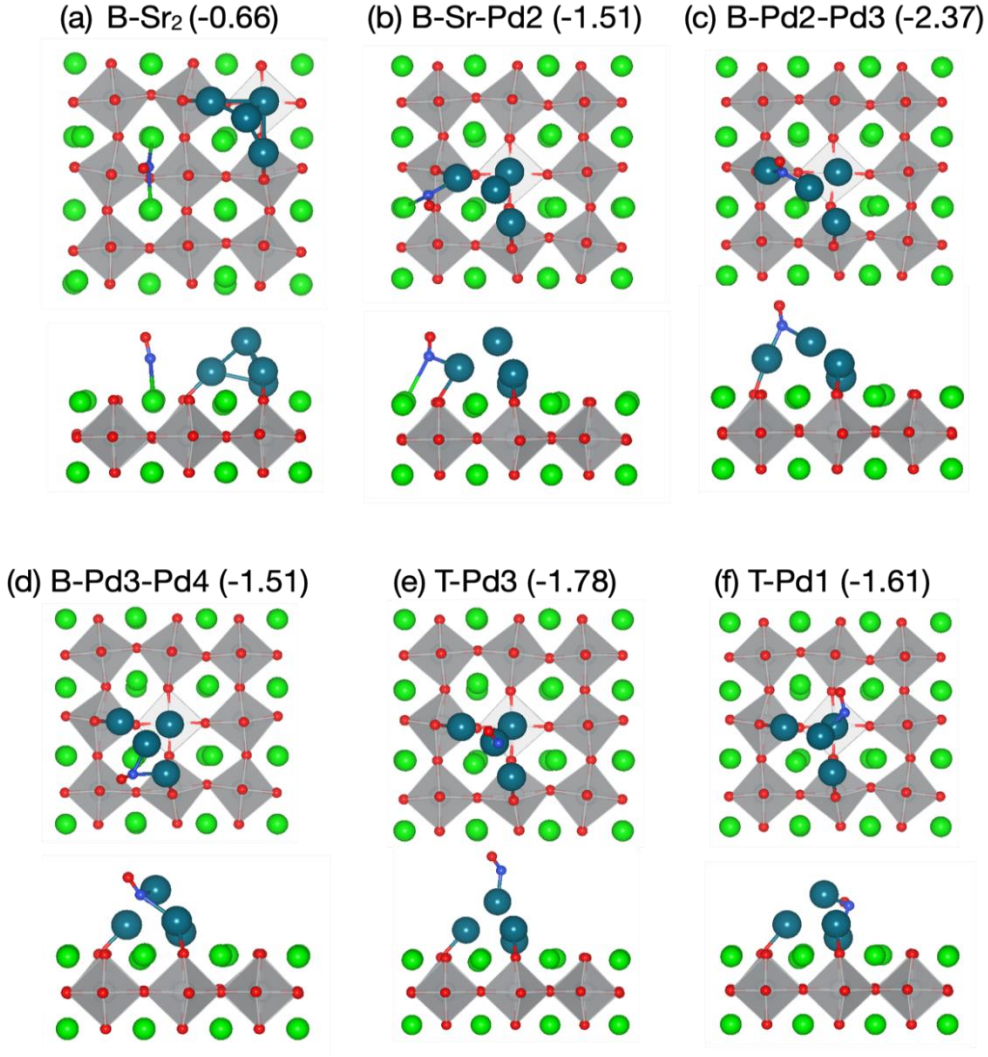


**Figure 2. Top and side views of single NO adsorbed on the $Pd_4/STO+V_O$ slab model with different adsorption sites. The value in parenthesis is the NO adsorption energy in eV. the N atom is represented by a blue ball stick**

We are now addressing the NO adsorption on $Pd_4/STO+V_O$. We load a single NO molecule to $Pd_4/STO+V_O$ in several adsorption sites and geometries. The structural optimization of $NO/Pd_4/STO+V_O$ is then performed and the NO adsorption energy is calculated by

$$E_{ads} = E(NO/Pd_4/STO + V_O) - E(Pd_4/STO + V_O) - E(NO), \quad (1)$$

Where $E$(NO/$Pd_4$/STO+$V_O$), $E$($Pd_4$/STO+$V_O$), and $E$(NO) are total DFT energies for single NO adsorbed on $Pd_4$/STO+$V_O$, pristine $Pd_4$/STO+$V_O$, and isolated NO molecule, respectively. The more negative the adsorption energy, the more energetically favorable or stable the adsorption of NO on the surface is.

The NO adsorption energy values ($E_{ads}$) range from −1.51 to −2.37 eV when NO is adsorbed on the supported $Pd_4$ cluster and at the interface region between $Pd_4$ and substrate (Figures 2b-f). In contrast, $E_{ads}$ of NO on the STO surface is only −0.66 eV (Figure 2a). This implies that NO tends to adsorbs on the Pd cluster or Pd-support interface rather than on STO surface. This is consistent with the fact that PGM nanoparticle is the active for the NO reduction reaction.

The most stable (preferred) NO adsorption site is the bridge site between the Pd2 and Pd3 atoms, denoted as B-Pd2-Pd3, with an adsorption energy ($E_{ads}$) of −2.37 eV (Figure 2c). In terms of stability, this is followed by T-Pd3 (−1.78 eV), T-Pd1 (−1.61 eV), and B-Pd3-Pd4 (−1.51 eV). Notably, NO tends to adsorb at a bridge site between an interface Pd atom and a non-interface Pd atom, rather than on top of a non-interface Pd atom. This suggests that electronic metal-support interaction, through electron donation from the STO support, plays a crucial role in tuning the NO adsorption site and strengthening the interaction of NO with the interface-noninterface Pd bridge site.

The N-O bond lengths in B-Pd2-Pd3, T-Pd3, T-Pd1, B-Pd3-Pd4 are 1.245, 1.189, 1.231, 1.158 Å, respectively. It appears that the N–O bond elongates upon adsorption on $Pd_4$/STO+VO due to the back-donation process (Pham et al., 2018, 2020, 2022). Moreover, at the most favorable adsorption site, the N–O bond undergoes the greatest elongation, indicating that the adsorbed NO is most effectively activated at this site and the bridge site between interface and noninterface Pd atoms could be the active site for the NO reduction reaction. Further theoretical research is necessary to fully elucidate the mechanism of NO activation and reaction.

### *3.3 Electronic structure analysis*

We now discuss the electronic structure of adsorbed NO at the most stable adsorption site, i.e., B-Pd2-Pd3. Charge density difference ($\Delta\rho$) is estimated as total electron density between NO/$Pd_4$/STO+$V_O$ and their fragments, namely NO and $Pd_4$/STO+$V_O$ and is shown in Figure 3. From the $\Delta\rho$ iso-surface (Figure 3a), it is clear that the electron redistribution cloud near the NO molecule reflects the $2\pi^*$ orbitals and electrons are depleted near Pd atoms, showing that the adsorption of NO on the supported $Pd_4$ is primarily governed via the hybridization between the Pd wave function and these orbitals. The $\Delta\rho$ profile along z direction in Figure 3(b) indicates that electron donation takes place from Pd atom to NO molecule, making NO become negatively-charged upon adsorption.

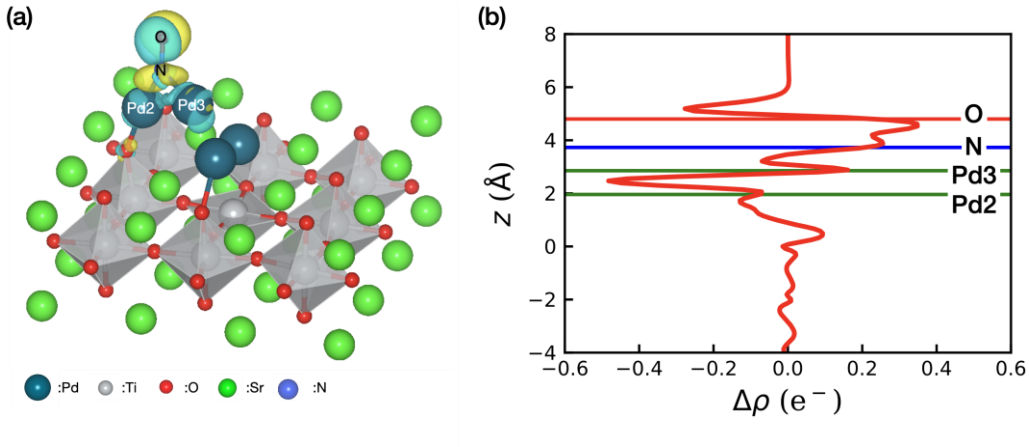


**Figure 3. (a) Charge density difference (Δ$\rho$) of the B-Pd2-Pd3 structure and (b) the integrated Δ$\rho$ along the *z* direction. The isosurface is plotted at 0.005 $e^-$/Bohr$^{-3}$, where yellow and cyan colors correspond to the electron accumulation and depletion, respectively**

We now discuss the electronic structure of adsorbed NO at the most stable adsorption site, i.e., B-Pd2-Pd3. The charge density difference (Δ$\rho$) is estimated as the total electron density between NO/$Pd_4$/STO+$V_O$ and their fragments, namely NO and $Pd_4$/STO+VO, as shown in Figure 3. From the Δ$\rho$ iso-surface (Figure 3a), it is evident that the electron redistribution cloud near the NO molecule reflects the 2π* orbitals, and electron depletion occurs near the Pd atoms. This indicates that the adsorption of NO on the supported $Pd_4$ is primarily governed by the hybridization between the Pd wave function and these orbitals. The Δ$\rho$ profile along the z-direction in Figure 3(b) suggests that electron donation occurs from the Pd atom to the NO molecule, causing NO to become negatively charged upon adsorption. The electron donation from Pd cluster to NO is further proved by the increase in the work function of $Pd_4$/STO+$V_O$. The calculated work functions of $Pd_4$/STO+$V_O$ with and without the NO adsorption are 3.68 and 3.32 eV, respectively.

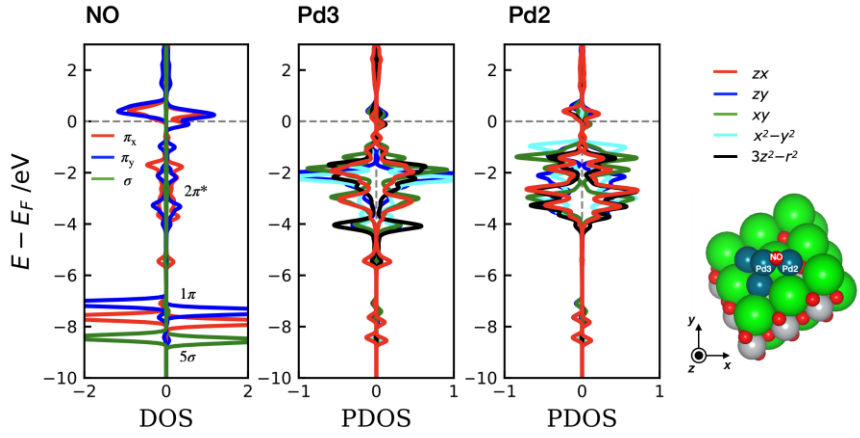


**Figure 4. Projected density of state (PDOS) for NO adsorbed on $Pd_4$/STO+$V_O$ at the most stable adsorption site, i.e., B-Pd2-Pd3. The local σ- and π-orbitals for NO of adsorbed NO are given in the text**

To gain more insight into the role of the hybridization between the NO molecular orbital and substrate wave functions in NO adsorption, projected density of state (PDOS) analysis for the adsorbed NO is then carried out. The PDOS of local σ- and π-orbitals for NO is estimated as

$$\pi_x = 2p_x(\mathrm{N}) + 2p_x(\mathrm{O})$$
$$\pi_y = 2p_y(\mathrm{N}) + 2p_y(\mathrm{O})$$
$$\sigma = 2p_z(\mathrm{N}) + 2p_z(\mathrm{O})$$

The PDOS for local σ- and π-orbitals of NO and for Pd atoms are shown in Figure 4. According to the Blyholder model, NO adsorption occurs via donation and back-donation processes (Pham et al., 2018, 2020, 2022). Donation involves the electron transfer from the occupied 1σ and 1π orbitals of NO to the empty or partially occupied orbitals of Pd atoms, while back-donation occurs when electrons from the occupied or partially occupied orbitals of Pd atoms are transferred to the 2π* orbitals of NO. The donation process is indicated by the resonance peaks in the PDOS between the 1σ and 1π orbitals of NO and Pd atoms, from $E_F - 9$ to $E_F - 5.8$ eV. In contrast, the back-donation process is evident from the downshift of the 2π* orbitals to lower energies, as well as from the interaction between the 2π* orbitals and Pd *d*-states, as indicated by the resonance peaks in the PDOS from $E_F - 5.5$ to $E_F + 1.0$ eV. We find that NO is negatively charged upon adsorption on $Pd_4/STO+V_O$, suggests a stronger back-donation from filled Pd *d*-states than the forward donation from the NO molecule.

Our calculations indicate that NO can strongly adsorb onto $Pd_4/STO+V_O$ via the back donation process. The electron donation to the antibonding 2π* orbitals of NO results in the N-O bond elongation, thereby weakening the N-O bond. In the future, we will thoroughly investigate the NO+CO reaction on $Pd_4/STO+V_O$ to gain a complete understanding of this reaction mechanism.

## 4. CONCLUSIONS

We have studied NO adsorption on $Pd_4/STO+V_O$ using density functional theory (DFT) calculations. Our findings show that NO is strongly adsorbed and activated on $Pd_4/STO+VO$ at the interface Pd atoms. Electronic structure analysis reveals that the strong NO adsorption originates from the 2π* back-donation process, facilitated by the hybridization of these molecular orbitals with Pd *d*-states. This work may contribute to the rational design of new $NO_x$ purification catalysts, potentially helping to mitigate environmental pollution and combat climate change.

## REFERENCES

Al Fauzan, M. R., Pham, T. N., Halim, H. H., Hamamoto, Y., Inagaki, K., Hamada, I., & Morikawa, Y. (2023). *First-Principles Microkinetic Study of NO Reduction on Cu Catalysts.* J. Phys. Chem C, 127(39), 19451–19467.

Beppu, K., Demizu, A., Hosokawa, S., Asakura, H., Teramura, K., & Tanaka, T. (2018). *Pd/SrFe1- xTixO3-δ as Environmental Catalyst: Purification of Automotive Exhaust Gases. ACS Appl. Mater. Inter*., 10(26), 22182–22189.

Demizu, A., Beppu, K., Hosokawa, S., Kato, K., Asakura, H., Teramura, K., & Tanaka, T. (2017). *Oxygen Storage Property and Chemical Stability of SrFe1-xTixO3-δ with Robust Perovskite Structure*. J. Phys. Chem C, 121(35), 19358–19364.

Fujiwara, A., Yoshida, H., Ohyama, J., & Machida, M. (2020). *Change in the Pd Oxidation State during Light-Off of Three-Way Catalysis Analyzed by in situ Diffuse Reflectance Spectroscopy*. J. Phys. Chem C, 124(23), 12531–12538.

Giannozzi, P., Andreussi, O., Brumme, T., Bunau, O., Nardelli, M. B., Calandra, M., Car, R., Cavazzoni, C., Ceresoli, D., Cococcioni, M., & others. (2017). *Advanced capabilities for materials modelling with Quantum ESPRESSO*. J. Phys. Condens. Matter, 29(46), 465901.

Goodman, E. D., Johnston-Peck, A. C., Dietze, E. M., Wrasman, C. J., Hoffman, A. S., Abild-Pedersen, F., Bare, S. R., Plessow, P. N., & Cargnello, M. (2019). *Catalyst deactivation via decomposition into single atoms and the role of metal loading.* Nat. Catal., 2(9), 748–755.

Granger, P., & Parvulescu, V. I. (2011). *Catalytic NOx Abatement Systems for Mobile Sources: From Three-Way to Lean Burn after-Treatment Technologies*. Chem. Rev., 111(5), 3155–3207.

Grimme, S., Antony, J., Ehrlich, S., & Krieg, H. (2010*). A consistent and accurate ab initio parametrization of density functional dispersion correction (DFT-D) for the 94 elements H-Pu*. J. Chem. Phys., 132(15).

Hammer, B., Hansen, L. B., & Nørskov, J. K. (1999). *Improved adsorption energetics within density-functional theory using revised Perdew-Burke-Ernzerhof functionals*. Phys. Rev. B, 59(11), 7413–7421.

Hirakawa, T., Shimokawa, Y., Miyahara, Y., Tsushida, M., Yoshida, H., Ohyama, J., & Machida, M. (2021). *Activity–composition relationships of Fe–Ni–Cu ternary nanoparticles supported on Al2O3 as three-way catalysts for NO reduction*. ACS Appl. Nano Mater., 4(10), 10613–10622.

Lammel, G., & Graßl, H. (1995). *Greenhouse effect of NOX. Environ*. Sci. Pollut. Res. Int., 2(1), 40–45.

Otani, M., & Sugino, O. (2006*). First-principles calculations of charged surfaces and interfaces: a plane-wave nonrepeated slab approach.* Phys. Rev. B, 73(11), 115407.

Pham, T. N., Andrea Choi Tan, B., Hamamoto, Y., Inagaki, K., Hamada, I., & Morikawa, Y. (2024). *Stability of PdxOy Particles Supported on Strontium Titanate Perovskite under Three-Way Catalyst Operating Conditions: Implications for Sintering Resistance.* ACS Catal., 14(3), 1443–1458.

Pham, T. N., Hamamoto, Y., Inagaki, K., Hamada, I., & Morikawa, Y. (2022). *Density functional theory study of NO-H2O coadsorption on Cu* (111). Phys. Rev. Mater., 6(7), 75801.

Pham, T. N., Hamamoto, Y., Inagaki, K., Son, D. N., Hamada, I., & Morikawa, Y. (2020). *Insight into trimeric formation of nitric oxide on Cu*(111): a density functional theory study. J. Phys. Chem. C, 124(5), 2968–2977.

Pham, T. N., Sugiyama, M., Muttaqien, F., Putra, S. E. M., Inagaki, K., Son, D. N., Hamamoto, Y., Hamada, I., & Morikawa, Y. (2018). *Hydrogen bond-induced nitric oxide dissociation on cu* (110). J. Phys. Chem. C, 122(22), 11814–11824.

Spezzati, G., Su, Y., Hofmann, J. P., Benavidez, A. D., DeLaRiva, A. T., McCabe, J., Datye, A. K., & Hensen, E. J. M. (2017). *Atomically dispersed Pd-O species on CeO2*(111) as highly active sites for low-temperature CO oxidation. ACS Catal., 7(10), 6887–6891.

Su, Y. Q., Liu, J. X., Filot, I. A. W., & Hensen, E. J. M. (2017). *Theoretical Study of Ripening Mechanisms of Pd Clusters on Ceria*. Chem. Mater., 29(21), 9456–9462.

Vanderbilt, D. (1990). *Soft self-consistent pseudopotentials in a generalized eigenvalue formalism*. Phys. Rev. B, 41(11), 7892.

Wang, J., Yang, J., Opitz, A. K., Bowman, W., Bliem, R., Dimitrakopoulos, G., Nenning, A., Waluyo, I., Hunt, A., Gallet, J. J., & Yildiz, B. (2021). *Tuning point defects by elastic strain modulates nanoparticle exsolution on perovskite oxides*. Chem. Mater., 33(13), 5021–5034.